AFM-based spherical indentation of a brush-coated soft material

Argatov, Ivan; Jin, Xiaoqing; Mishuris, Gennady

Published in:
Soft Matter

DOI:
10.1039/d3sm00432e

Publication date:
2023

Citation for published version (APA):
Argatov, I., Jin, X., & Mishuris, G. (2023). AFM-based spherical indentation of a brush-coated soft material: Modeling the bottom effect. *Soft Matter*, *19*(26), 4891-4898. https://doi.org/10.1039/d3sm00432e

M-based spherical indentation of a brush-coated soft material: deling the bottom effect

Argatov,[ab] Xiaoqing Jin*[a] and Gennady Mishuris[c]

s a common practice in the atomic force microscopy (AFM)-based studies of living cells to entiate them by values of the elastic (Young's) modulus, which is supposed to be an effective acteristic of the mechanical properties of a cell as a heterogeneous matter. The elastic response cell to AFM indentation is known to be affected by a relative distance from the AFM probe ne solid support on to which the cell is cultured. Besides this so-called bottom effect, AFM surements may carry significant information regarding the effect of molecular brushes covering g cells. Here, we develop a mathematical model for determining the intrinsic effective Young's ulus of a single brush-coated cell from the force-indentation curve with the bottom effect taken account. The mathematical model is illustrated on the example of AFM data on testing of an ryotic cell taken from the literature.

1 Introduction

Living cells are well known as fundamental units of living organisms [1,2], and many pathological diseases can be directly caused by irregular cellular mechanics [3,4]. How physical forces and mechanical properties of cells contribute to cell development, physiology and disease is a primary focus of mechanobiology [5], whereas atomic force microscopy (AFM) [6,7] provides a variety of quantitative single-cell methods and techniques [4] for probing mechanical properties at the micro-and nanoscale.

In the contact (static) mode of AFM, an AFM probe (indenter) attached to the free end of an AFM cantilever is indented into a tested cell sample, and the contact force, F, is recorded as being proportional to the cantilever deflection. By standard processing [6] of the AFM raw data, including the height position of the piezoelectric translator that controls the position of the fixed end of the AFM cantilever, the corresponding indenter displacement, δ, can be determined starting from the contact point where $F = 0$ and $\delta = 0$. Thus, recorded upon approaching, the force-displacement curve (F vs. δ) provides a characteristic of the mechanical response of the cell sample under indentation.

So, given the force-displacement curve, the problem is to extract viable information about the cell mechanobiology. This crucially depends [4,5] on the choice of an appropriate indentation model $F(\delta)$, which is determined by the following main aspects:

- Indenter geometry;
- Constitutive model (elastic, viscoelastic, etc.);
- Loading protocol;
- Geometry of cell (thickness/bottom effect);
- Substrate and environment effects;
- Indenter/cell contact interface (adhesion, friction, brush coating layer).

In AFM studies of both soft biological tissues and living cells [8,9], different types of probe geometries are used, among them, spherical probes. In what follows, we consider, namely, the case of a spherical indenter, which is characterized by the indenter radius, R_{probe}. In applications to soft tissues, the contact deformations of the AFM probe (which is usually made from a much stiffer material), as a rule, can be neglected.

The choice of the constitutive model strongly depends on the type of cell [5,10]. In the majority of studies, the linear elasticity theory is assumed, and the simple effective model of an isotropic homogeneous elastic material for the cell body is adopted. In what follows, we make use of the linearly-elastic constitutive model, which also serves as a basic model [11] for the introduction of viscoelastic [12,13] and poroelastic [14] effects. Usually the assumption of incompressibility is utilized ($\nu_{\mathrm{cell}} = 0.5$), as the effective Poisson's ratio ν_{cell} of the cell body is close to 0.5 but it is difficult to be evaluated precisely.

The geometry of the cell sample is critically important factor for an appropriate mathematical modeling of the force-displacement relation, which, however, is rarely taken into account explicitly [16,17]. In the overwhelming majority of studies, the condition of axisymmetry is employed to simplify the indentation model. When approximating the cell's surface, which is entering into contact with the AFM probe (see Fig. 1), by a smooth surface with some local radius of curvature, R_{cell}, the contact development can be characterized by the radius of the contact zone, a, and the contact stiffness depends on the ratio between a and R_{cell}. Strictly

[a] College of Aerospace Engineering, Chongqing University, Chongqing, 400030, China; E-mail: jinxq@cqu.edu.cn.
[b] Institut für Mechanik, Technische Universität Berlin, 10623 Berlin, Germany.
[c] Department of Mathematics, Aberystwyth University, Ceredigion SY23 3BZ, Wales, UK.

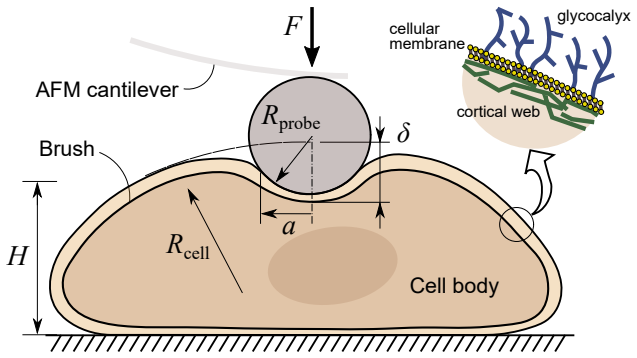

Fig. 1 Schematic of the AFM-based indentation of a living cell cultured on a rigid support, illustrating the mechanical structure of a pericellular coat (after[15]).

speaking, the contact radius a does depend on the level of contact loading, which is directly influenced not only by the contact force F but also is restricted by the indenter radius, R_{probe}.

The classical model of Hertz (see, e.g.,[18]) assumes that $a \ll R_{\text{cell}}$ and predicts the following force-displacement relation for an absolutely rigid spherical indenter (whose shape is approximated by a paraboloid):

$$F = \frac{4}{3} E^* \sqrt{R} \delta^{3/2}. \tag{1}$$

Here, E^* is the so-called reduced elastic modulus, which is related to the effective elastic modulus of cell, E_{cell}, by the formula $E^* = E_{\text{cell}}/(1-\nu_{\text{cell}}^2)$, and R is the effective curvature radius defined as $R = R_{\text{probe}} R_{\text{cell}}/(R_{\text{probe}} + R_{\text{cell}})$. It is to be remembered that the axisymmetric Hertz theory also provides the following estimate for the contact radius: $a = \sqrt{R\delta}$. Given the geometrical parameter R, the Hertzian equation (1) can be used for determining the elastic constant E^* by fitting to the experimentally measured function $F(\delta)$.

It is well known that the Hertz theory does not account for the effect of finite contact geometry, and as such, the so-called bottom effect[19,20] (or the effect of the sample thickness beneath the indenter[21,22]) is completely neglected in the Hertz model (1). It has been recognized[22,23] that the strength of the bottom/thickness effect is governed by the relation between the contact radius a and the sample thickness H (see Fig. 1). Obviously, the Hertzian equation (1) is strictly valid only when $a \ll H$.

The generalizations of the Hertz model (1) for the bottom effect in AFM measurements, which were derived by Dimitriadis *et al.*[24] and Garcia and Garcia[23], can be represented in the form

$$F = \frac{4}{3} E^* \sqrt{R} \delta^{3/2} f(\varpi), \tag{2}$$

where we have introduced the notation

$$\varpi = \frac{\sqrt{R\delta}}{H}. \tag{3}$$

The correction factor $f(\varpi)$ admits the asymptotic-like expansion

$$f(\varpi) \simeq 1 + C_1\varpi + C_2\varpi^2 + C_3\varpi^3 + C_4\varpi^4, \tag{4}$$

where the coefficients $C_1, \ldots, C_4$ depend on the boundary conditions at the bottom surface, as it has been shown elsewhere[25,26].

The accuracy of the analytical approximations of the power-series type (4) has been recently investigated by Hermanowicz[27] who obtained the approximate force-displacement relations for paraboloidal, conical, and cylindrical indenters in the cases of unbonded and bonded incompressible elastic layers, which are valid in the whole range of variation of the relative indentation $R\delta/H^2 = \varpi^2$. As the matter of fact, the simple power series asymptotic expansion (4) can be used with a less than 5% error for relatively thick samples, when the contact diameter $2a$ does not exceed the sample thickness, i.e., for $a/H \le 0.5$.

The bottom effect reveals itself in deviations of the experimental force-displacement curve from Hertz's 3/2-power law (1). In particular, when the Hertzian equation (1) is applied to fitting the force-displacement curve whose trend follows Eq. (2), the obtained results will expose a growing tendency for the apparent reduced elastic modulus. This fact is illustrated in Fig. 2 in dimensionless variables.

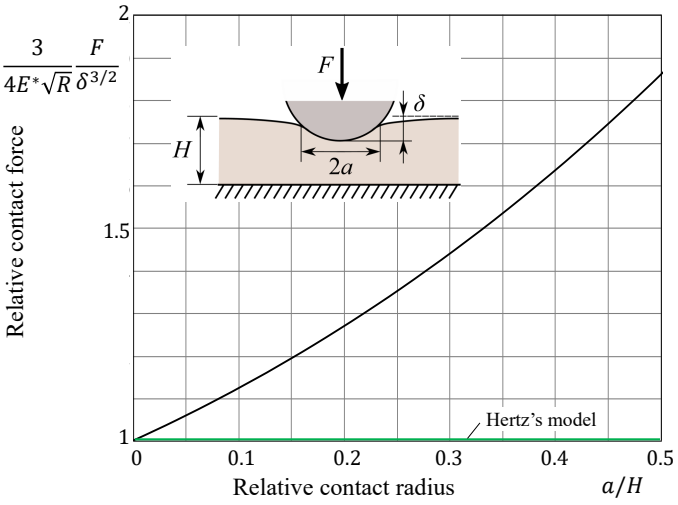

Fig. 2 The bottom effect in spherical (paraboloidal) frictionless indentation of an incompressible linearly-elastic layer bonded to a rigid base.

There are different issues regarding the substrate effects. In particular, the substrate's stiffness can be relatively low to consider the support (base) as absolutely rigid[28]. The effect of the stiffness of a semi-infinite (elastic half-space) can be taken into account by means of formula (4) with appropriate coefficients (see[26] for details). The effect of the substrate prestress can be regarded as an active factor of loading[29]. The so-called corrugated substrates[30] are used to facilitate a stable position for a loosely fixed cell (see also[31]).

Further, the development of an appropriate indentation model strongly depends on the physical effects associated with the indenter/cell contact interface. While the effects of indenter surface roughness and friction usually can be neglected in AFM measurements of living cells, the effect of adhesion, if it is strong enough, should be taken into account[32,33]. For soft biological tissues, the Johnson–Kendall–Roberts (JKR) model[34] is commonly applied, and its generalization for accounting the bottom effect similar to the asymptotic expansion (2) was produced in[35].

Finally, the so-called interface deformation effects can be associated either with the membrane tension[36,37] or the contact deformation of a pericellular coat[38,39]. The most external glycocalyx compartment (cell coat) is determined by the length, density and internal structure of this brush like overlayer of proteoglycans and glycoproteins[15]. The proteoglycan composition of the brush layer varies according to the cell type as well as its thickness (from about one hundred nanometers to a few micrometers)[40]. Using AFM indentation testing with relatively large spherical probes, it is possible to assess only a homogenized (or averaged) stiffness property of the pericellular coat, without nanomechanical profiling its long-branched carbohydrate chains (see Fig. 1). Recently, the analysis of the robustness of the brush model[38,39] has been analyzed[41] based on a variety of AFM force curves obtained from different types of cells adhered tightly to the bottom of cell culture dishes.

An open question remains how to account for both the effect of pericellular brush and the bottom effect. In the present study, we build upon our prior work[42] and develop the fourth-order asymptotic approximation for the bottom effect in the brush/cell model.

2 Theory

2.1 Indentation problem formulation

We consider an elastic layer of thickness H bonded to a rigid base and covered with a brush-like layer of thickness L (see Fig. 3a). The two-layer system is referred to a cylindrical coordinate system (r,z), such that the horizontal plane $z=0$ coincides with the brush/layer interface and the vertical z-axis is pointed downwards inside the layer. In the unloaded state (see Fig. 3a), the surface of an axisymmetric rigid spherical indenter of radius R is supposed to be in a point contact with the top surface of the brush, so that the initial gap between these two surfaces is given by

$$\Phi(r)=\frac{r^2}{2R}. \tag{5}$$

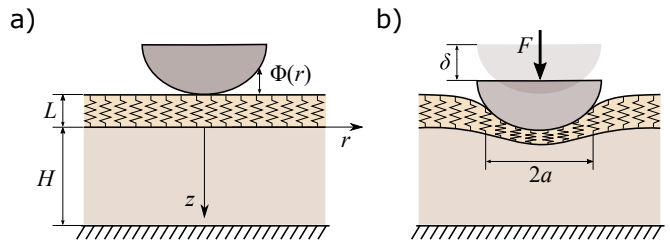

Fig. 3 Schematic of the unilateral contact between a rigid probe and a brush-covered elastic layer: a) Unloaded state with a single point contact; b) Loaded state with contact over a circular area.

In the loaded state (see Fig. 3b), the indenter being acted upon by an external force F establishes contact over a circular zone of radius a and receives some vertical displacement δ. If the contact force F is regarded as an independent variable, then both the indenter displacement δ and the contact radius a will be single-valued functions of F. The displacement-force relation (δ vs. F) or the force-displacement relation (F vs. δ) depends on the mechanical response to indentation of both components of the two-layer system.

In many studies on AFM measurements of living cells, the model of a homogeneous elastic layer is assumed for the cell body[7]. As such, the principle of superposition applies and the normal (vertical) displacements of the layer's top surface due to the action of the normal surface tractions distributed over a circular area of radius a with an axisymmetric density $p(r)$ can be expressed as follows[43]:

$$u_z(r)=\frac{1}{\pi E^* H}\int\limits_0^{2\pi}\mathrm{d}\phi\int\limits_0^{a}K\big(H^{-1}\sqrt{r^2+\rho^2-2r\rho\cos\phi}\big)p(\rho)\rho\,\mathrm{d}\rho. \tag{6}$$

Here, E^* is the so-called reduced elastic modulus, ρ and ϕ are the polar variables of integration, and the function

$$G_z(r)=\frac{1}{\pi E^* H}K\Big(\frac{r}{H}\Big) \tag{7}$$

determines the surface influence function with a source at the center of coordinates. In other words, the kernel $K(t)$ in the double integral (6) is a dimensionless function of a dimensionless argument $t\in(0,+\infty)$, which is related to the surface Green's function (7).

Using the Fourier transform (see, e.g.,[44]), the following integral representation can be established[43]:

$$K(t)=\int\limits_0^{\infty}L(u)J_0(ut)\,\mathrm{d}u. \tag{8}$$

Here, $J_0(x)$ is the Bessel function of the first kind, and L is a kernel function, which can be expressed in a simple explicit analytical form, depending on the boundary conditions imposed on the layer's bottom surface.

Following[42], the deformation response to indentation of the brush coating will be modeled according to the nonlinear Winkler-type model

$$p=p_1 f\Big(\frac{D}{L}\Big),\quad 0<D\le L, \tag{9}$$

where the prefactor p_1 is a constant having a physical dimension of pressure, $f(\lambda)$ is a positive strictly monotonically decreasing function such that $f(1)=0$ and $f(\lambda)\to+\infty$ as $\lambda\to 0$, D is the local deformed thickness of the brush coating, and $\lambda=D/L$ is the local stretch ratio.

In the framework of the Alexander–de Gennes (AdG) theory[45,46], we have $f(\lambda)=f_{\mathrm{AdG}}(\lambda)$, where

$$f_{\mathrm{AdG}}(\lambda)=\lambda^{-9/4}-\lambda^{3/4}. \tag{10}$$

It should be noted[41] that accounting for adhesive effects would require a modification of the AdG model. Also, two brush lengths of significantly different densities are required[47] to generalize the exponential approximate form[48] of the AdG model for pathological cells.

Since the brush does not transfer any shear loading, the condition of static equilibrium in the vertical direction (see Fig. 4)

implies that

$$F = 2\pi \int_0^a p(r) r \, \mathrm{d}r, \tag{11}$$

where $p(r)$ is the *a priori* unknown contact pressure density, which describes the distributed surface tractions on both surfaces of the brush layer.

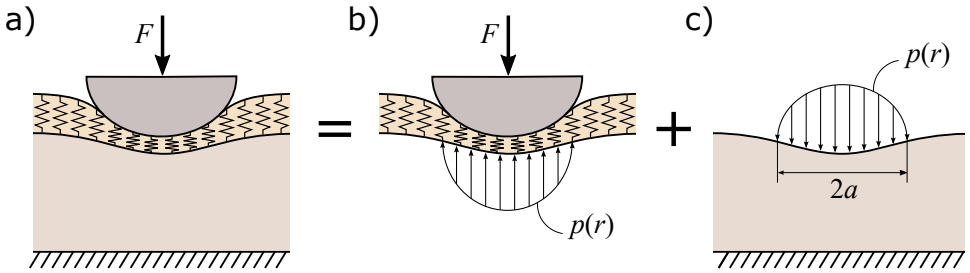

Fig. 4 Schematic of the two-layer system equilibrium: a) The loaded state; b) The brush is compressed between the indenter and the elastic layer; c) The elastic layer is subject to surface tractions only beneath the indenter.

In order to formulate the governing integral equation that determines the function $p(r)$, $r \in [0,a]$, we consider the kinematic contact condition that embodies a balance of the vertical displacements in the two-layer system in the loaded state. With this aim we recall that in the unloaded state (see Fig. 3a) there is the variable initial gap $\Phi(r)$ between the indenter surface and the brush surface, which should vanish if the indenter surface comes into contact with the brush.

In the loaded state, the indenter receives some vertical displacement, so that the two surfaces establish full contact inside the contact zone (see Fig. 5b). The deformed thickness of the brush layer becomes $D(r)$, whereas the variable layer thickness will be equal to $H-u_z(r)$, taking into account the nonlinear and linear responses of the brush and the layer, respectively. As a result, the total variable thickness of the deformed two-layer system will be

$$D(r)+\big(H-u_z(r)\big)=L+H-\big(\delta-\Phi(r)\big), \tag{12}$$

where the right-hand side gives the distance between the indenter surface (in the loaded state) and the rigid base.

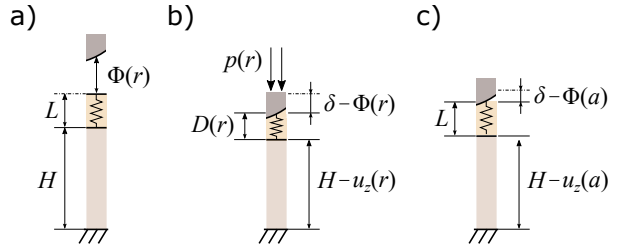

Fig. 5 Schematic of the contact deformation in the two-layer system: a) The unloaded state; b) The loaded state; c) The loaded state at the contact contour.

Finally, if we consider the contact condition at the contour of the contact area (see Fig. 5c), we find that

$$p(a)=0, \tag{13}$$

$$D(a)=L, \tag{14}$$

under the assumption that there is no adhesion between the indenter surface and the brush coating, so that the indenter can produce only positive pressures inside the contact zone, i.e., $p(r)>0$ for $r\in[0,a)$.

So, in view of the constitutive equation (9), we have

$$D(r)=Lf^{-1}\left(\frac{p(r)}{p_1}\right), \tag{15}$$

where $f^{-1}(\cdot)$ is the inverse constitutive function of the brush model.

Then, the substitution of (6) and (15) into Eq. (12) yields

$$L\left\{1-f^{-1}\left(\frac{p(r)}{p_1}\right)\right\}+\frac{1}{\pi E^*}\big(\mathscr{G}p\big)(r)=\delta-\Phi(r), \tag{16}$$

where we have introduced the notation

$$\big(\mathscr{G}p\big)(r)=\frac{1}{H}\int_0^{2\pi}\mathrm{d}\phi\int_0^a K\big(H^{-1}\sqrt{r^2+\rho^2-2r\rho\cos\phi}\big)p(\rho)\rho\,\mathrm{d}\rho. \tag{17}$$

The governing integral equation (16) differs from that derived in[42] by the integral operator (17), which now incorporates the bottom effect.

2.2 Asymptotic models

It is well known that the Green's function (7) is singular function, as it describes the elastic layer's response to a point force loading. In the case of an elastic layer, it admits the asymptotic expansion

$$G_z(r)=\frac{1}{\pi E^*}\frac{1}{r}-\frac{1}{\pi E^* H}\left\{a_0+a_1\frac{r^2}{H^2}+\ldots\right\}, \tag{18}$$

where $a_0,a_1,\ldots$ are the so-called asymptotic constants, which depend on the type of boundary conditions on the layer bottom surface.

Based on the asymptotic properties of the kernel function in the integral representation (8), it can be shown[43] that the power series in (18) is absolutely convergent for $r<2H$. This means that while approximating the surface influence function $G_z(r)$ by truncated power series of the type (18), it is possible to get reliable results only for relatively thick layers, i.e., for small values of the ratio a/H.

By retaining two terms in (18), that is, by using only the first two asymptotic constants a_0 and a_1, we can construct the fourth-order asymptotic model (see[25]). In this way (see[26] for details), the integral operator (17) is approximated as

$$\big(\mathscr{G}p\big)(r)\simeq\big(\mathscr{B}p\big)(r)-\frac{a_0}{H}F-\frac{a_1}{H^3}r^2F, \tag{19}$$

where $\big(\mathscr{B}p\big)(r)$ is the Boussinesq's integral operator, which in the axisymmetric case is defined as

$$\big(\mathscr{B}p\big)(r)=4\int_0^a \mathbf{K}\left(\frac{2\sqrt{\rho r}}{\rho+r}\right)\frac{p(\rho)\rho}{(r+\rho)}\,\mathrm{d}\rho. \tag{20}$$

Here, $\mathbf{K}(x)$ is the complete elliptic integral of the first kind.

Thus, the substitution of (19) into Eq. (16) yields the following approximate governing integral equation:

$$L\left\{1-f^{-1}\left(\frac{p(r)}{p_1}\right)\right\}+\frac{1}{\pi E^*}\big(\mathscr{B}p\big)(r) = \delta+\frac{a_0}{H}\frac{F}{\pi E^*} + \frac{a_1}{H^3}\frac{F}{\pi E^*}r^2-\Phi(r). \tag{21}$$

Observe that in the case of a spherical (paraboloidal) indenter (with the shape function being defined by Eq. (5)), the right-hand side of Eq. (21) is of the quadratic form $c_0+c_1r^2$, where c_0 and c_1 are constants with respect to r, and thus, Eq. (21) is of the same type as that solved approximately in[42].

2.3 Approximate displacement-force relation

Following[42], we approximate the contact pressure by the Hertz solution

$$p(r)=\frac{3F}{2\pi a^2}\sqrt{1-\frac{r^2}{a^2}}, \tag{22}$$

and substituting (22) into Eq. (21), we reinforce the obtained approximate relation at the points $r=0$ and $r=a$ to derive the

two coupled approximate equations

$$L\left\{1-f^{-1}\left(\frac{3F}{2\pi a^2 p_1}\right)\right\}+\frac{3F}{8E^*a}=\frac{a^2}{2R}-\frac{a_1}{H^3}\frac{a^2F}{\pi E^*}, \tag{23}$$

$$\frac{3F}{8E^*a}+\frac{a^2}{2R}-\frac{a_1}{H^3}\frac{a^2F}{\pi E^*}=\delta+\frac{a_0}{H}\frac{F}{\pi E^*}. \tag{24}$$

We note that the second-order asymptotic model for the bottom effect is obtained by keeping only one asymptotic constant a_0, when Eqs. (23) and (24) simplify as

$$L\left\{1-f^{-1}\left(\frac{3F}{2\pi a^2 p_1}\right)\right\}+\frac{3F}{8E^*a}=\frac{a^2}{2R}, \tag{25}$$

$$\frac{3F}{8E^*a}+\frac{a^2}{2R}=\delta+\frac{a_0}{H}\frac{F}{\pi E^*}. \tag{26}$$

It should be emphasized that in the limit as L tends to zero or p_1 tends to infinity, Eqs. (23), (24) and Eqs. (25), (26) result in the fourth- and second-order asymptotic models for an elastic layer without any coating[25].

It is readily seen that Eq. (24) as well as Eq. (26) can be easily resolved for the indenter displacement δ in terms of the contact force F and the contact radius a. However, it is not possible to resolve for a neither Eq. (23) nor Eq. (25). That is why, Eqs. (23), (24) provide the displacement-force relations in *implicit* form. The same, of course, concerns Eqs. (25), (26) of the somewhat more simple model.

3 Results

3.1 Indentation model in the nondimensionalized form

Following[42], we introduce the dimensionless variables

$$\bar{a}=\frac{a}{R},\quad \bar{\delta}=\frac{\delta}{R},\quad \bar{F}=\frac{3F}{8E^*R^2} \tag{27}$$

and the dimensionless parameters

$$\bar{L}=\frac{L}{R},\quad \bar{H}=\frac{H}{R},\quad \chi^*=\frac{4E^*}{\pi p_1}. \tag{28}$$

Moreover, to simplify the formulas, we put

$$\alpha_0=\frac{8a_0}{3\pi},\quad \alpha_1=-\frac{8a_1}{3\pi}. \tag{29}$$

Then, Eqs. (23) and (24), respectively, can be rewritten as

$$\chi^*\frac{\bar{F}}{\bar{a}^2}=f\left(1-\frac{\bar{a}^2}{2\bar{L}}+\frac{\bar{F}}{\bar{a}\bar{L}}-\alpha_1\frac{\bar{F}\bar{a}^2}{\bar{L}\bar{H}^3}\right), \tag{30}$$

$$\bar{\delta}=\frac{\bar{F}}{\bar{a}}+\frac{\bar{a}^2}{2}-\alpha_0\frac{\bar{F}}{\bar{H}}+\alpha_1\frac{\bar{F}\bar{a}^2}{\bar{H}^3}. \tag{31}$$

Evidently, the second-order asymptotic model in the nondimensionalized form is recovered from Eqs. (30), (31) by neglecting the terms with α_1.

3.2 Fitting the model to experimental data

Let $\mathscr{A}(\bar{F},\chi^*)$ denote the solution of Eq. (30) with respect to $\bar{a}$, that is

$$\bar{a}=\mathscr{A}(\bar{F},\chi^*). \tag{32}$$

Then, the substitution of (32) into Eq. (31) yields

$$\bar{\delta}=\mathscr{D}(\bar{F},\chi^*), \tag{33}$$

where we have introduced the notation

$$\mathscr{D}(\bar{F},\chi^*) = \frac{\bar{F}}{\mathscr{A}(\bar{F},\chi^*)}-\alpha_0\frac{\bar{F}}{\bar{H}} + [\mathscr{A}(\bar{F},\chi^*)]^2\left(\frac{1}{2}+\alpha_1\frac{\bar{F}}{\bar{H}^3}\right). \tag{34}$$

Thus, evaluating the nondimensionalized displacement-force relation (33) requires the numerical solution of Eq. (30).

In order to fit a given set of experimental data (i.e., a discrete set of values of the indenter displacement δ corresponding to a discrete set of values of the contact force F) by making use of the indentation-force relation in the non-dimensionalized form (33), we introduce a *dimensional* scaling parameter F_1. In this way, the dimensional form of the indentation-force relation can be represented as

$$\delta=R\mathscr{D}\left(\frac{F}{F_1},\chi^*\right). \tag{35}$$

It should be underlined that, in view of (30) and (34), the function on the right-hand side of Eq. (35) also depends on the dimensionless geometrical parameters $\bar{L}$ and $\bar{H}$, which either assumed to be known *a priori* or can be evaluated in the process of fitting.

After determining the fitting parameters F_1 and χ^*, we make use of the third formulas in (27) and (28) to evaluate the effective reduced elastic modulus

$$E^*=\frac{3F_1}{8R^2} \tag{36}$$

and the brush stiffness parameter

$$p_1=\frac{4E^*}{\pi\chi^*}, \tag{37}$$

where E^* is given by (36).

It should be also remembered that, generally speaking, the asymptotic constants α_0 and α_1 depend on the layer Poisson's ratio, which is also supposed to be known in advance.

3.3 Illustrative example

We consider the same example as that considered previously in[42], which is based on the AFM data on indentation of an eukaryotic cell with a 5 μm spherical probe (silica particle) taken from[39]. The cell thickness parameter H was estimated as 10 μm based on the heights of cells between 10 and 20 μm reported in[49] for firmly and loosely adhered cells.

We recall that usually[50] living cells are assumed to be incompressible, that is $\nu_{\text{cell}}=0.5$. However, this assumption should be regarded as an oversimplification, which is usually made due to the lack of a more reliable information. For instance, the Poisson's ratio of chondrocytes (cells within articular cartilage) was found to be 0.38[51]. In this study, following[52], we assume that $\nu_{\text{cell}}=0.4$, and thus we will have $\alpha_0=1.28912$ and $\alpha_1=0.63454$ (see Supplementary Information). The effect of the local curvature of the cell at the indentation center is neglected due to the lack of infor-

mation, so that we put $R = R_{\text{probe}}$, where $R_{\text{probe}} = 5\ \mu$m.

The AdG model (10) is adopted as the brush model, and the average value $L = 2.36\ \mu$m for the brush thickness is fixed based on the data reported in [38]. The only other brush parameter p_1 is set to be free (it enters the nondimensionalized model equations via the dimensionless parameter χ^*).

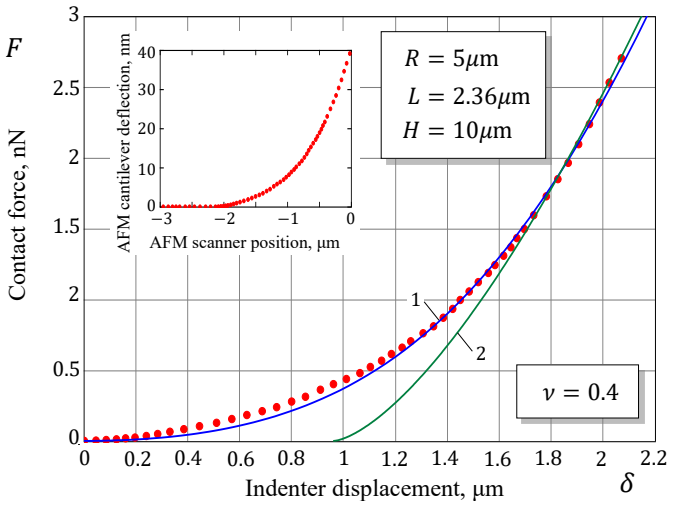

Fig. 6 An example of processing raw data [39] (see the insert), deflection of the AFM cantilever versus vertical position of the AFM scanner (red dotted line). Solid lines 1 and 2 respectively denote the present model (blue line, 1) and the Hertz model (green line, 2).

Based on the refined brush/cell model (30), (31) (with the asymptotic constants α_0 and α_1 given above and corresponding to the case of a compressible bonded layer) the following fitting results have been obtained (see Fig. 6): $E_1 = 435.9$ Pa, $p_1 = 9.13$ Pa, and $\chi^* = 72.39$. It should be noted that since the constructed model possesses a higher accuracy for the advanced stage of indentation, the emphasis in fitting the processed experimental AFM data was put on the range $F \geq 0.6$ nN, thereby increasing the accuracy of determination of the cell reduced elastic modulus E^*.

The Hertzian fit of the advanced part of the force-displacement curve is also shown in Fig. 6. The corresponding estimate for the cell Young's modulus is $E_2 = 656.86$ Pa, which is almost 50% larger than E_1. This is clearly explained by the manifestation of the bottom effect.

4 Discussion

First of all, we would like to draw attention to the importance of the bottom effect. As it can be seen from Fig. 2, the Hertz model provides a less than 5% error when $a/H \leq 0.05$, which approximately corresponds to the range $\varpi \leq 0.05$ (for the paraboloidal frictionless indentation of a bonded incompressible layer). In a quite common situation, when the contact diameter does not exceed the sample thickness at the center of indentation, the difference can be almost two-fold and dramatically increases with the increase of the ratio a/H above 0.5 (see also [22,27]).

When the bottom effect is neglected (this may happen, e.g., due to the lack of information regarding the contact thickness, that is the thickness of a tested cell sample at the point of indentation), the obtained AFM results may be misinterpreted. For instance, the Hertz model-based analysis of dynamic spherical AFM indentation study on cardiomyocytes [53] shows that cells are softer at the nuclear region and become stiffer toward the periphery [4], which apparently is also a demonstration of the bottom effect.

It should be emphasized [22,23] that namely the ratio a/H governs the strength of the bottom effect. It is usually assumed [4,54] that the bottom (thickness) effect can be neglected if the AFM tip is not indented by more than 10% of the cell thickness. However, this simple esimate should be used with caution. Indeed, according to Eqs. (3) and (2), the bottom effect is a function of the dimensionless parameter ϖ, which is a product of two dimensionless factors $\sqrt{\delta/H}$ and $\sqrt{R/H}$. As such, for any given value of the level of indentation (defined by the ratio δ/H), the bottom effect will still depend on the relative size of the AFM probe (determined by the ratio R/H).

Observe that the layer thickness parameter H can be canceled in Eq. (12). This means that the kinematic contact condition (12) can be equivalently derived from the consideration of the variable brush thickness only. As such, the governing integral equation (16) also applies in the case of a cell attached to an elastic substrate, which can be modeled as an elastic half-space, using Burmister's solution for the surface influence function [55]. Correspondingly, the asymptotic models (21) and (23)–(26) still can be utilized provided the asymptotic constants a_0 and a_1 are evaluated using the kernel function recovered from Burmister's solution (see [56] for details).

In the example considered above (spherical probe made of silica), the neglection of the indenter deformations is completely justified by a seven order-of-magnitude ratio $E_{\text{probe}}/E_{\text{cell}}$ of the indenter and cell moduli. However, generally speaking, the incorporation of the effect of indenter elasticity into the brush/cell model is quite straightforward and this can be done by means of the so-called effective (composite) elastic modulus as in the Hertz theory [18], though the contact between the indenter and the cell body occurs via the brush layer.

In order to account for the bottom effect in AFM indentation, one needs to know not only an experimental force curve but also the geometric parameters (including, the brush thickness L and the cell thickness H) — the latter information, which is prerequisite to the application of the described models, is difficult to collect and usually absent in the overwhelming majority of studies.

Finally, while in the engineering contact mechanics [18] (see also [11]), the error of the paraboloidal approximation (5) for the spherical surfaces in local contact is generally regarded as very small in the range of infinitesimally small contact deformations, it makes sense to develop a generalization of the indentation model for a spherical indenter (using the exact indenter geometry [26,57]), since the brush layer experiences relatively large compressive deformations in the contact zone. This issue requires a separate study.

5 Conclusions

It has been highlighted that the strength of the bottom/substrate effect strongly depends on the size of the contact area compared to the contact thickness of the cell sample. The asymptotic modeling method, which has been applied for incorporating the bottom effect into the brush/cell model, allows not only to account for different boundary conditions at the bottom surface but also, *per se*, to incorporate the substrate effect, when the asymptotic constants are appropriately evaluated from the corresponding surface influence function.

Author Contributions

I.A. and X.J. worked on model derivation and drafted the manuscript. G.M. contributed to the discussion and interpretation of the results. I.A. and X.J. edited the paper. All authors discussed the results, reviewed the manuscript, and approved the final version.

Declaration of Interests

The authors declare no competing interests.

Acknowledgment

This work is supported by the National Science Foundation of China (Grant Nos. 11932004 and 51875059). X.J. would like to acknowledge the support from Chongqing City Science and Technology Program (Grant No. cstc2020jcyj-msxmX0850). G.M. is thankful to the Royal Society for the Wolfson Research Merit Award and Sêr Cymru Future Generations Industrial Fellowship. I.A. is grateful to the financial support from the Ba-Yu Scholar program of Chongqing City (China).

Notes and references

1 C. M. O'Connor, J. U. Adams and J. Fairman, *Essentials of Cell Biology*, NPG Education, Cambridge, MA, 2010.

2 M. L. Rodriguez, P. J. McGarry and N. J. Sniadecki, *Applied Mechanics Reviews*, 2013, **65**, 060801.

3 D. Ingber, *Annals of Medicine*, 2003, **35**, 564–577.

4 C. T. Mierke, in *Physics of Cancer*, IOP Publishing, Bristol, 2018, ch. Cell–cell and cell–matrix adhesion strength, local cell stiffness and forces, pp. 4–1–4–60.

5 M. Krieg, G. Fläschner, D. Alsteens, B. M. Gaub, W. H. Roos, G. J. Wuite, H. E. Gaub, C. Gerber, Y. F. Dufrêne and D. J. Müller, *Nature Reviews Physics*, 2019, **1**, 41–57.

6 H.-J. Butt, B. Cappella and M. Kappl, *Surface Science Reports*, 2005, **59**, 1–152.

7 R. Garcia, *Chemical Society Reviews*, 2020, **49**, 5850–5884.

8 M. E. Dokukin and I. Sokolov, *Macromolecules*, 2012, **45**, 4277–4288.

9 I. Sokolov, in *Contact Problems for Soft, Biological and Bioinspired Materials*, ed. F. M. Borodich and X. Jin, Springer International Publishing, Cham, 2022, ch. Contact problem in indentation measurements of soft, biological and bioinspired materials, pp. 31–49.

10 B. R. Brückner and A. Janshoff, *Biochimica et Biophysica Acta (BBA)-Molecular Cell Research*, 2015, **1853**, 3075–3082.

11 I. Argatov and G. Mishuris, *Indentation Testing of Biological Materials*, Springer, Cham, 2018.

12 Y. M. Efremov, W.-H. Wang, S. D. Hardy, R. L. Geahlen and A. Raman, *Scientific Reports*, 2017, **7**, 1–14.

13 P. D. Garcia and R. Garcia, *Nanoscale*, 2018, **10**, 19799–19809.

14 E. Moeendarbary, L. Valon, M. Fritzsche, A. R. Harris, D. A. Moulding, A. J. Thrasher, E. Stride, L. Mahadevan and G. T. Charras, *Nature Materials*, 2013, **12**, 253–261.

15 M. Szymonski, M. Targosz-Korecka and K. E. Malek-Zietek, *Pharmacological Reports*, 2015, **67**, 728–735.

16 Y. Ding, G.-K. Xu and G.-F. Wang, *Scientific Reports*, 2017, **7**, 45575.

17 J. Rheinlaender, A. Dimitracopoulos, B. Wallmeyer, N. M. Kronenberg, K. J. Chalut, M. C. Gather, T. Betz, G. Charras and K. Franze, *Nature Materials*, 2020, **19**, 1019–1025.

18 K. L. Johnson, *Contact Mechanics*, Cambridge University Press, Cambridge, 1987.

19 N. Gavara and R. S. Chadwick, *Nature Nanotechnology*, 2012, **7**, 733–736.

20 S. Chiodini, S. Ruiz-Rincón, P. D. Garcia, S. Martin, K. Kettelhoit, I. Armenia, D. B. Werz and P. Cea, *Small*, 2020, **16**, 2000269.

21 W. C. Hayes, L. M. Keer, G. Herrmann and L. F. Mockros, *Journal of Biomechanics*, 1972, **5**, 541–551.

22 I. Argatov, A. U. Daniels, G. Mishuris, S. Ronken and D. Wirz, *European Journal of Mechanics-A/Solids*, 2013, **37**, 304–317.

23 P. D. Garcia and R. Garcia, *Biophysical Journal*, 2018, **114**, 2923–2932.

24 E. K. Dimitriadis, F. Horkay, J. Maresca, B. Kachar and R. S. Chadwick, *Biophysical Journal*, 2002, **82**, 2798–2810.

25 I. I. Argatov, *International Journal of Solids and Structures*, 2011, **48**, 3444–3452.

26 I. I. Argatov and F. J. Sabina, *Quarterly Journal of Mechanics and Applied Mathematics*, 2013, **66**, 75–95.

27 P. Hermanowicz, *International Journal of Mechanical Sciences*, 2021, **193**, 106138.

28 B. L. Doss, K. R. Eliato, K.-h. Lin and R. Ros, *Soft Matter*, 2019, **15**, 1776–1784.

29 J. F. Waters, J. Kalow, H. Gao and P. R. Guduru, *Journal of Adhesion*, 2012, **88**, 134–144.

30 M. Hernando-Perez, C. Zeng, L. Delalande, I. Tsvetkova, A. Bousquet, M. Tayachi-Pigeonnat, R. Temam and B. Dragnea, *Journal of Physical Chemistry B*, 2016, **120**, 340–347.

31 I. Argatov and X. Jin, *International Journal of Engineering Science*, 2020, **154**, 103349.

32 S. Sen, S. Subramanian and D. E. Discher, *Biophysical Journal*, 2005, **89**, 3203–3213.

33 X. Zhu, E. Siamantouras, K. K. Liu and X. Liu, *Journal of the Mechanical Behavior of Biomedical Materials*, 2016, **56**, 77–86.

34 K. L. Johnson, K. Kendall and A. D. Roberts, *Proceedings of the Royal Society of London. A.*, 1971, **324**, 301–313.

35 I. I. Argatov, F. M. Borodich and V. L. Popov, *Journal of Physics D: Applied Physics*, 2015, **49**, 045307.

36 R. W. Style, C. Hyland, R. Boltyanskiy, J. S. Wettlaufer and E. R. Dufresne, *Nature Communications*, 2013, **4**, 1–6.

37 Y. Ding, J. Wang, G.-K. Xu and G.-F. Wang, *Soft Matter*, 2018, **14**, 7534–7541.

38 I. Sokolov, S. Iyer, V. Subba-Rao, R. M. Gaikwad and C. D. Woodworth, *Applied Physics Letters*, 2007, **91**, 023902.

39 I. Sokolov and M. E. Dokukin, in *Nanoscale Imaging: Methods and Protocols*, ed. Y. L. Lyubchenko, Springer New York, New York, NY, 2018, ch. AFM indentation analysis of cells to study cell mechanics and pericellular coat, pp. 449–468.

40 S. Marcotti and G. C. Reilly, *Mechanobiology: Exploitation for Medical Benefit*, 2017, 43–60.

41 N. Makarova and I. Sokolov, *Nanoscale*, 2022, **14**, 4334–4347.

42 I. Argatov, X. Jin and G. Mishuris, *Journal of the Royal Society Interface*, 2023, 20220857.

43 A. M. Alexandrov and D. A. Pozharskii, *Three-Dimensional Contact Problems*, Kluwer, Dordrecht, 2001.

44 I. N. Sneddon, *Fourier transforms*, McGraw-Hill, New York, 1951.

45 S. Alexander, *Journal De Physique*, 1977, **38**, 983–987.

46 P. G. de Gennes, *Advances in Colloid and Interface Science*, 1987, **27**, 189–209.

47 S. Iyer, R. M. Gaikwad, V. Subba-Rao, C. D. Woodworth and I. Sokolov, *Nature Nanotechnology*, 2009, **4**, 389–393.

48 J. N. Israelachvili, *Intermolecular and Surface Forces*, Academic Press, New York, 1992.

49 M. E. Dokukin, N. V. Guz and I. Sokolov, *Biophysical Journal*, 2013, **104**, 2123–2131.

50 C. T. Lim, E. H. Zhou and S. T. Quek, *Journal of Biomechanics*, 2006, **39**, 195–216.

51 W. R. Trickey, F. P. Baaijens, T. A. Laursen, L. G. Alexopoulos and F. Guilak, *Journal of Biomechanics*, 2006, **39**, 78–87.

52 R. E. Mahaffy, S. Park, E. Gerde, J. Käs and C.-K. Shih, *Biophysical Journal*, 2004, **86**, 1777–1793.

53 S. G. Shroff, D. R. Saner and R. Lal, *American Journal of Physiology-Cell Physiology*, 1995, **269**, C286–C292.

54 A. B. Mathur, A. M. Collinsworth, W. M. Reichert, W. E. Kraus and G. A. Truskey, *Journal of Biomechanics*, 2001, **34**, 1545–1553.

55 D. M. Burmister, *Journal of Applied Physics*, 1945, **16**, 89–94.

56 I. Argatov, *Mechanics of Materials*, 2010, **42**, 807–815.

57 A. H. England, *Mathematical Proceedings of the Cambridge Philosophical Society*, 1962, **58**, 539–547.